Acoustic emission-driven fractal analysis for damage warning in FRP-strengthened corroded RC beams

Pan, Tanbo; Xu, Xubing; Zheng, Yonglai; Wu, Liangqin; Yang, Chao; Aydin, Beyazit Bestami; Li, Yang; Zhou, Yubao

DOI
10.1016/j.engfracmech.2025.111563

Publication date
2025

Document Version
Final published version

Published in
Engineering Fracture Mechanics

Citation (APA)
Pan, T., Xu, X., Zheng, Y., Wu, L., Yang, C., Aydin, B. B., Li, Y., & Zhou, Y. (2025). Acoustic emission-driven fractal analysis for damage warning in FRP-strengthened corroded RC beams. *Engineering Fracture Mechanics*, *328*, Article 111563. https://doi.org/10.1016/j.engfracmech.2025.111563

Engineering Fracture Mechanics 328 (2025) 111563

Contents lists available at ScienceDirect

Engineering Fracture Mechanics

journal homepage: www.elsevier.com/locate/engfracmech

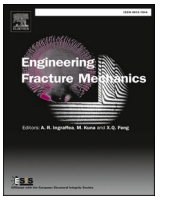

Acoustic emission-driven fractal analysis for damage warning in FRP-strengthened corroded RC beams

Tanbo Pan [a], Xubing Xu [b,*], Yonglai Zheng [b], Liangqin Wu [a], Chao Yang [a], Beyazit Bestami Aydin [c], Yang Li [d], Yubao Zhou [e]

[a] College of Civil Engineering and Architecture, East China Jiaotong University, China
[b] Department of Hydraulic Engineering, College of Civil Engineering, Tongji University, China
[c] Department of Civil Engineering, Middle East Technical University (METU), Turkey
[d] Kunming Institute of Physics, China
[e] Faculty of Civil Engineering and Geosciences, Delft Univerisity of Technology, Netherlands

ARTICLE INFO

Keywords:
Acoustic emission
Corrosion
Damage assessment
Damage warning
Reinforced concrete (RC) beam
Fractal analysis

ABSTRACT

This study introduces a novel approach that integrates Acoustic Emission monitoring with fractal analysis to assess and predict damage progression in FRP-strengthened reinforced concrete beams subjected to corrosion-induced deterioration. By combining AE signals with fractal measures, specifically the correlation dimension, the research provides an effective tool for tracking internal damage evolution and offering early-warning indicators for structural health. The developed damage model identifies three distinct stages of damage: initial damage, damage evolution, and sustained growth. The study reveals that corrosion accelerates both the accumulation and rate of damage, with AE ring counts significantly increasing in moderately to severely corroded beams, indicating heightened crack activity and reduced structural capacity. The correlation dimension shows a strong relationship with the degree of damage, with higher values corresponding to more disordered internal damage. The correlation dimension evolves from an initial increase to a decrease as damage progresses, marking the transition from early to advanced degradation. These findings highlight that corrosion not only accelerates damage but also lowers the detection threshold for significant structural damage.

1. Introduction

Reinforced concrete structures are the backbone of urban infrastructure, but their durability is severely degraded by internal reinforcement corrosion, leading to performance deterioration and safety hazard. There is an urgent need to develop effective real-time damage monitoring technologies [1–3]. The use of Fiber Reinforced Polymer (FRP) composites for the rehabilitation and strengthening of deteriorating RC structures has gained considerable attention in recent decades. This is primarily due to the superior mechanical properties of FRP materials, including high strength-to-weight ratios, corrosion resistance, and ease of application [4–8]. These attributes make FRP an ideal candidate for enhancing the structural performance of RC members, particularly those subjected to corrosion-induced damage. Despite its advantages, one of the most critical challenges faced in the application of FRP in strengthening schemes is the premature debonding of FRP sheets from the concrete substrate [9,10]. This failure mode often occurs at significantly

* Corresponding author.
E-mail address: xxb@tongji.edu.cn (X. Xu).

https://doi.org/10.1016/j.engfracmech.2025.111563
Received 23 May 2025; Received in revised form 3 September 2025; Accepted 16 September 2025
Available online 17 September 2025

lower strain levels than the ultimate tensile strength of the FRP, reducing the efficiency and durability of the reinforcement system. To address this challenge, FRP anchorage systems have been developed to prevent or delay the premature debonding of FRP sheets. These anchorage systems, which can be integrated with existing FRP strengthening techniques, offer an innovative solution by enhancing the bond between the FRP and the concrete, ensuring a more reliable transfer of stress across the interface [11–13]. Compared to traditional reinforcement methods, FRP anchoring systems offer significant advantages. First, steel anchors are prone to corrosion and have poor long-term durability. Second, while CFRP U-shaped stirrups are corrosion-resistant, their ends are susceptible to stress concentration issues, which can impair load-bearing performance. Third, the near-surface embedding (NSE) method requires complex wet operations, making construction cumbersome and causing significant disruption to existing structures. In contrast, FRP anchoring systems are completely non-metallic and corrosion-resistant, can deform in coordination with FRP panels and concrete substrates, and can be installed with only surface bonding or shallow embedding. This feature is particularly suitable for existing structures that need to maintain operations or require minimal disruption during reinforcement [14,15].

FRP anchorage system, typically composed of FRP sheets and anchors, significantly enhance the performance of concrete structures, particularly in extending the lifespan of aging infrastructure. However, the interaction between FRP and concrete, along with the dynamic behavior under load, introduces complex failure mechanisms that are challenging to monitor with traditional methods. To assess the structural integrity of FRP-strengthened RC beams, it is essential to understand the damage evolution within these composite systems. Acoustic emission (AE) technology offers a powerful solution for real-time, non-invasive monitoring by detecting high-frequency elastic waves generated by internal damage [16–22]. AE enables continuous tracking of damage initiation and progression, providing valuable insights into the performance of the FRP layers, anchors, and concrete substrate [23–25]. Several studies have demonstrated the effectiveness of acoustic emission in real-time, non-invasive monitoring of internal damage in FRP-repaired or reinforced concrete cylinders under various loading conditions. Ma et al. [26,27] used AE to track crack evolution in BFRP-repaired concrete cylinders under axial compression, employing advanced analysis methods to classify crack types and monitor crack propagation. Liu et al. [28] found that increasing the number of FRP bonding layers enhanced peak load and AE signal intensity, with RA-AF and b-value parameters proving useful for evaluating damage. Du et al. [29] applied AE to FRP/steel–concrete hybrid girders, successfully distinguishing macro and microdamage and showing that cumulative AE energy correlates with local strain. Therefore, the AE technique is a widely used approach for monitoring damage progression in RC structures.

Fractal theory has emerged as a powerful tool for analyzing nonlinear systems, particularly in mechanics and solid-state physics, over the past three decades [30–32]. Unlike traditional B-value analysis, which primarily focuses on the statistical distribution of amplitude in acoustic emission events, fractal analysis originates from the theory of complex systems in nonlinear science. It views material damage and failure as a dynamic fractal structure evolving in space and time. The novelty of this method lies in its approach to acoustic emission events not as independent statistical samples but as a unified whole, quantifying the complexity and clustering patterns of their spatial distribution or time series. By calculating the evolution curve of the fractal dimension, we can sensitively capture the critical phase transition point where the internal damage mechanisms of the material transition from random, disordered microcrack initiation to ordered, localized macrocrack propagation [33–35]. As a result, fractal analysis of AE signals provides an effective method for monitoring the damage evolution in materials. Ye et al. [36] used multifractal theory to analyze the AE characteristics of anisotropic shale under direct shear, demonstrating that the variations in fractal dimension and the width of the multifractal spectrum could effectively explain the asymmetric failure behavior. Kong et al. [37] explored the time-varying characteristics of AE signals and fractal behavior during coal's structural failure under uniaxial compression. The study found that the AE energy signals exhibited strong fractal characteristics, with the information dimension following a dynamic "increase-decrease-increase" pattern, where a rapid decrease in the dimension served as an effective precursor to predicting coal failure. Yang et al. [38] studied the fractal dimension in shale with varying joint surfaces and sizes, finding that as joint surfaces and sample size increased, the fractal dimension decreased. This reduction in fractal dimension was linked to crack initiation and material failure. The study highlighted the

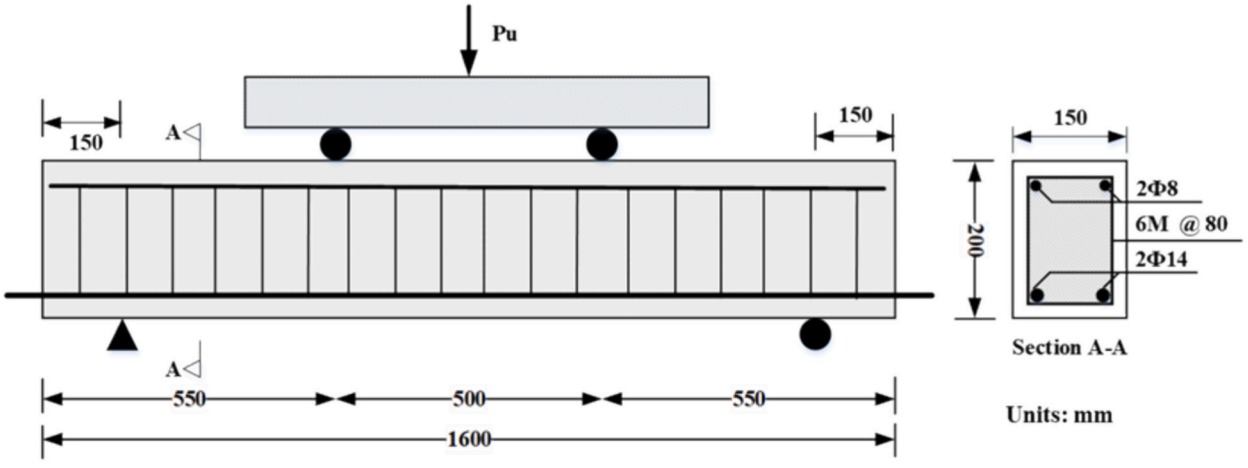

Fig. 1. Schematic diagram of specimen geometry and cross-section details.

importance of fractal dimension as a key indicator in predicting failure, with changes in fractal behavior serving as an early warning for instability in rock engineering. However, research on the fractal analysis of AE signals in FRP-strengthened corroded concrete beams is limited. Further exploration of quantitative multi-fractal analysis of AE parameters from fracture experiments is needed to enhance damage detection and early warning capabilities.

This study utilizes AE technology, combined with fractal analysis, to monitor the damage evolution of FRP-strengthened corroded RC beams. Four RC beams with varying degrees of corrosion (0 %, 5 %, 10 %, and 20 %) strengthened with FRP anchorage system were subjected to four-point bending tests to collect AE data. Based on the cumulative AE ringing counts, a damage evolution model for FRP-strengthened, corroded RC beams is proposed. Fractal analysis is then applied to the AE signals to explore the relationship between changes in fractal dimension and structural damage progression. Ultimately, this study aims to enhance the early warning capabilities for crack damage in FRP-strengthened, corrosion-damaged RC beams using AE-driven fractal analysis, providing a more precise damage prediction framework for structural health monitoring and assessment.

2. Experimental setup and data acquisition

2.1. Materials and specimens

The RC beams used in this study, as shown in Fig. 1, were designed to simulate typical structural configurations. Each beam measured 150 mm in width, 200 mm in depth, and 1600 mm in length. The concrete mix, with a volumetric ratio of 1:1.65:2.52 (cement:sand:aggregate) and a water-to-cement ratio of 0.47, was chosen to ensure suitable workability and strength. After standard curing, the beams achieved a 28-day compressive strength of 42.5 MPa (±3.6 MPa), typical for medium-strength concrete.

Reinforcement was provided through a combination of longitudinal and transverse steel bars. At the beam's bottom, two Φ14-HRB400 steel bars were placed to resist tensile forces, while two Φ8-HRB400 steel bars at the top ensured stability and compression resistance. Shear reinforcement consisted of Φ6-HRB400 stirrups spaced at 80 mm intervals, designed to resist shear stresses and secure the longitudinal bars. To enhance corrosion resistance, epoxy resin was applied at the intersections between stirrups and longitudinal reinforcement.

To further improve flexural performance, CFRP sheets were bonded to the beam's tensile face using epoxy adhesive. The CFRP sheets had a thickness of 1.02 mm, a tensile strength of 3000 MPa, and an elastic modulus of 230 GPa, with an ultimate strain of 1.66 %. The adhesive facilitated a robust bond between the CFRP sheets and the concrete surface, ensuring effective load transfer and reinforcement.

2.2. Accelerated corrosion testing setup

For the accelerated corrosion testing, a bespoke water tank was employed, containing a 5 % sodium chloride (NaCl) solution, which was placed beneath the cross-section of each beam to simulate a corrosive environment. The immersion period lasted for seven days, during which the concrete beams were exposed to the saltwater solution to initiate the corrosion process of the steel reinforcement. The climate chamber will maintain the ambient temperature at (22 ± 3)°C and the relative humidity at (63 ± 5)%.

After the initial immersion period, a stainless steel grid was installed close to the submerged segment's surface to serve as the cathode. The beam's longitudinal tensile reinforcement, connected to the positive terminal of a power supply, acted as the anode, while the stainless steel grid, connected to the negative terminal, ensured even distribution of corrosion across the span of the beam. This setup created a controlled electrochemical environment that mimicked the corrosion effects found in natural conditions. To maintain a consistent and uniform corrosion rate, the electrical current was set to 205 mA, resulting in an ampere density of 180 μA/cm^2. This current density was carefully regulated to ensure it did not exceed the threshold of 200 μA/cm^2, in line with best practices for simulating real-world corrosion without compromising the bond between the concrete and steel.

The corrosion process was carefully monitored using Faraday's second law of electrolysis (Eq. (1), which allows for the calculation of the theoretical mass loss of the tensile reinforcement during the corrosion process. The mass loss equation is given by:

$$Massloss = \frac{ItM}{Fn} \tag{1}$$

where I is the constant current (A), t is the corrosion duration (s), M is the atomic weight of iron (55.847 g/mol), F is Faraday's constant (96485C/mol), and n is the ion charge.

Based on this calculation, the beams were categorized into three levels of corrosion damage: mild (5 %), moderate (10 %), and severe (20 %), achieved after 25, 50, and 100 days of accelerated corrosion exposure, respectively. These corrosion levels provided the necessary variation to assess the impact of different extents of reinforcement degradation on the performance of the FRP-strengthened RC beams.

2.3. CFRP anchorage system strengthening

2.3.1. CFRP anchors construction

After the accelerated corrosion stage was completed, the anchor reinforcement process was subsequently carried out. The CFRP anchorage system was designed to enhance the flexural performance and durability of RC structures through a well-defined

construction process and standardized strengthening procedure. The CFRP anchorage system consists of customized anchors, constructed to maximize bonding efficiency and load transfer, and a precise installation method to ensure optimal reinforcement effectiveness.

The construction of the CFRP anchors begins with the selection of unidirectional CFRP sheets, cut to a standard width of 150 mm and length of 80 mm. The 80 mm length is divided into two sections: a 50 mm fan-shaped segment serving as the main anchor body and a 30 mm pre-formed section designed for a 90-degree bend. A 10 mm dowel is embedded within the fan-shaped section to establish structural integrity. To minimize stress concentration and prevent fiber damage, epoxy resin is applied over a 10 mm length at the sheet end, forming a hardened shaft. The 30 mm pre-formed section facilitates a flexible transition zone between the hardened portion and the main body, allowing for a controlled bend without compromising the anchor's integrity. Two CFRP sheets of different lengths are ultimately combined to produce a bow-tie-shaped anchor, which offers enhanced anchorage performance by balancing stiffness and flexibility. The fabrication process of FRP anchors is shown in Fig. 2.

2.3.2. *Strengthening procedure*

The CFRP anchorage system strengthening procedure was illustrated in Fig. 3. The strengthening procedure focuses on achieving strong bonding between the CFRP system and the concrete substrate while ensuring precise installation of the anchorage components. The process begins with surface preparation of the concrete beam using a pneumatic needle scaler to remove the surface layer and expose the aggregate, enhancing the mechanical interlock and adhesive properties of the interface. Subsequently, drilling is performed to create four holes, each 10 mm in diameter and 35 mm deep, at designated locations on the beam's bottom face. The holes are carefully marked, drilled, and cleaned using pressurized air and vacuum equipment to eliminate dust and debris, ensuring an uncontaminated bond for the epoxy adhesive.

Following surface preparation, epoxy resin application is carried out, where the resin is evenly spread along the prepared concrete surface and in alignment with the texture direction of the CFRP sheets. The CFRP sheets are immediately adhered to the surface, with a roller used to eliminate air pockets and ensure uniform coverage. The pre-fabricated CFRP anchors are then inserted into the pre-drilled holes, with a small amount of epoxy applied to the anchor rods to secure a strong bond within the holes. The anchorage depth and the protruding section of the anchors are meticulously controlled to maintain consistency and performance.

The entire CFRP system undergoes a curing period of seven days to allow the epoxy resin to achieve its full strength as specified by the manufacturer. During this period, the bond between the CFRP components and the concrete substrate is fully developed, ensuring the anchorage system's long-term structural integrity and load-bearing capacity.

2.4. *Load testing set-up*

The load testing was conducted using an electro-hydraulic servo testing machine with a maximum load capacity of 2000 kN. To ensure precise contact between the loading apparatus and the RC beam, two pre-loading cycles were performed prior to the formal test. The pre-load was set to 5 % of the theoretical ultimate load of the beam, ensuring optimal alignment and eliminating potential inaccuracies due to poor contact. During the formal loading phase, a displacement-controlled loading scheme was employed, with a constant loading rate of 1 mm/min applied until failure occurred. This rate was selected to replicate real-world loading conditions.

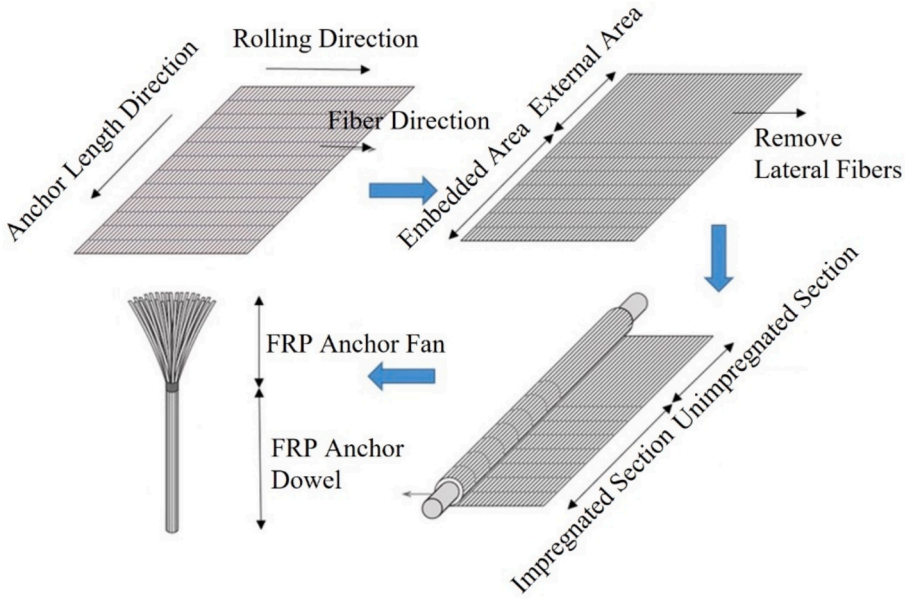

Fig. 2. The fabrication process of FRP anchors.

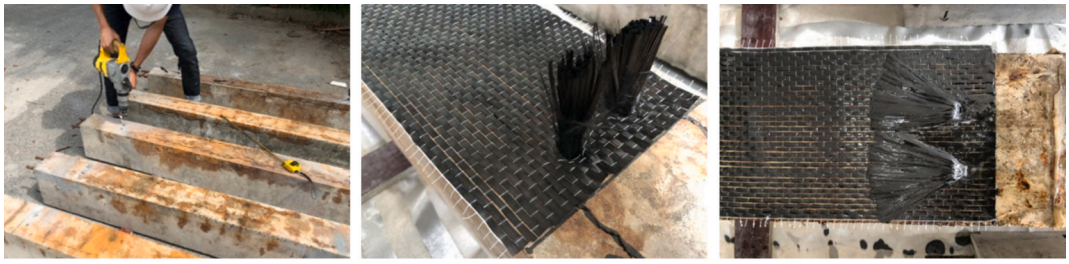

Fig. 3. Anchors installation procedure.

Throughout the test, high-definition cameras were positioned on both sides of the beam to monitor the progression of cracks and to document the beam's failure mode. These visual recordings provided critical data for subsequent analysis, offering a detailed understanding of the fracture mechanisms at play. The experimental setup, including the configuration of the loading device, is illustrated in Fig. 4.

2.5. AE system and measurement

AE signals were captured using the Micro-II digital AE system (Physical Acoustics Corporation), with real-time data monitoring and storage facilitated by AEwin software. Five AE sensors were mounted on each specimen, ensuring secure contact with the surface via silicon grease. The sensor positions are on the same side as shown in Fig. 5. Before the actual AE monitoring commenced, the sensitivity of the AE sensors underwent verification using a pencil lead break test according to E976-99 standard issued by American Society for Testing and Materials. The signal acquisition settings are summarized in Table 1. Key parameters include a lower filter of 20 kHz, a higher filter of 400 kHz, and specific times for peak definition (300 μs), hit definition (600 μs), and hit lockout (1000 μs). In addition, the threshold was set at 40 dB based on pre-tests, which demonstrated that this value can efficiently filter out ambient noise while remaining low enough to ensure that genuine cracking signals are not missed. These settings collectively optimize the detection and interpretation of relevant AE signals.

2.6. AE data filtering

To ensure the extraction of genuine AE hits while suppressing environmental noise and reflection artifacts during the loading of FRP-strengthened corroded beams, the following two-stage filtering procedure was employed. First, a hardware band-pass filter between 20 kHz and 400 kHz was applied in the AEwin system, with a constant threshold of 40 dB to reject low-level background noise.

Fig. 4. Diagram of the loading device.

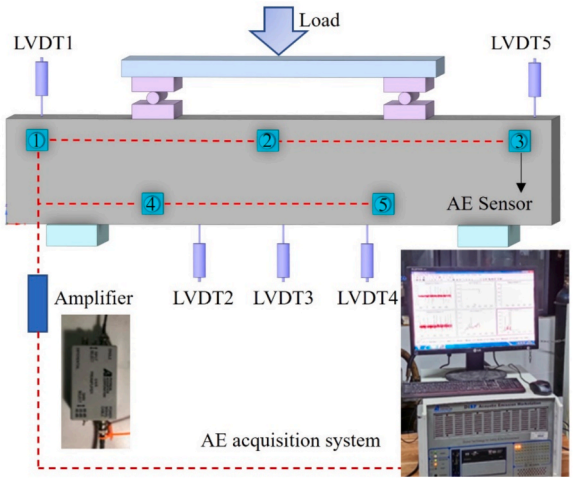

Fig. 5. Schematic diagram of sensor arrangement.

Table 1
AE signal collection setup.

Threshold (dB)	Higher filter (kHz)	Lower filter (kHz)	Peak definition time (μs)	Hit definition time (μs)	Hit lockout time (μs)
40	400	20	300	600	1000

Thereafter, a Swansong II amplitude–duration filter was implemented: recorded hits were sorted into ten discrete amplitude bands, each associated with a maximum permissible duration; any pulse exceeding its band-specific duration limit was discarded as spurious [39,40]. This dual filtering scheme effectively removes both high-amplitude/short-duration and low-amplitude/long-duration artefacts, thereby retaining only valid AE events for subsequent fractal-based damage analysis, as shown in Table 2.

3. Results of mechanical properties

3.1. Load capacity

Fig. 6 presents the load–deflection curves for CFRP-strengthened beams subjected to four-point bending. Table 3 provides a summary of the yield load P_y and ultimate load P_u of all specimen beams. Notably, the flexural behavior of the CFRP-strengthened beams displayed a consistent trend, closely linked to the extent of accelerated corrosion, or the corrosion level of the specimen beams. Specifically, the yield load of CS-5, CS-10, and CS-20 decreases by 12 %, 23 %, and 19 %, respectively, relative to the pristine beam (US-0). A similar trend is observed for the ultimate load, with reductions of 6.0 %, 14 %, and 22 %. Notably, as corrosion severity increases, the disparity in load-bearing capacity between adjacent specimens diminishes, particularly between CS-10 and CS-20. This indicates an accelerated degradation mechanism at higher corrosion levels, where the combined effects of reinforcement section loss and bond deterioration dominate the structural response.

Table 2
Duration-Amplitude Filter (Swansong II).

Condition	Amplitude (dB)	Duration (μs)
1	40–45	<500
2	46–49	<650
3	50–53	<820
4	54–56	<940
5	57–60	<1000
6	60–67	<2000
7	68–75	<4000
8	76–83	<6000
9	84–91	< 8000
10	92–100	< 10,000

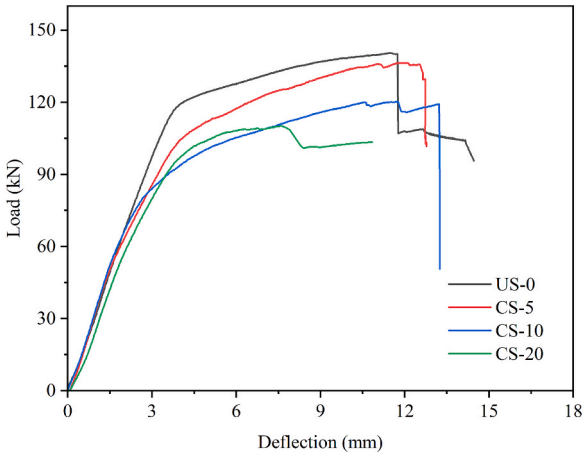

Fig. 6. Load–deflection curves of specimen.

Table 3
Summary of the test results.

Beams	P_y(kN)	P_u(kN)	$P_{y_{Nor}}$[a](kN)	$P_{u_{Nor}}$[a](kN)	Mode of failure
US-0	119.5	140.5	1.00	1.00	CCS
CS-5	104.8	131.4	0.88	0.94	CD-AP
CS-10	92.6	121.2	0.77	0.86	CD-AP
CS-20	97.0	109.8	0.81	0.78	MC-FT

[a]Normalized in relation to the beam US-0.

3.2. Failure modes

Fig. 7 illustrates the three principal failure modes observed in CFRP-strengthened beams subjected to four-point bending, highlighting the influence of corrosion severity on the structural response. The failure modes include concrete cover separation (CCS), CFRP-concrete debonding with anchor pull-out (CD-AP), and matrix cracking with fiber tearing (MC-FT), each corresponding to beams with varying corrosion levels.

Concrete cover separation (CCS), shown in Fig. 7 (a), occurred in the pristine beam (US-0) and was characterized by extensive spalling of the concrete cover at the beam's bottom. Notably, no debonding was observed between the CFRP sheet and the concrete substrate. This brittle failure behavior likely resulted from the effects of flexural cracks, leading to the detachment of the concrete cover. In contrast, the CD-AP failure mode, depicted in Fig. 7 (b), was identified in beams with light to moderate corrosion levels (CS-5 and CS-10). This mode involved CFRP-concrete interfacial debonding near the sheet's end, followed by the pull-out of anchor systems, often accompanied by local concrete cone failure. The debonding was primarily initiated by the propagation of flexural cracks into the substrate, coupled with relative displacement between the CFRP sheet and the concrete matrix. The anchors played a critical role in delaying complete debonding, transitioning the failure process from abrupt concrete cover separation to a more gradual debonding mechanism. This resulted in improved ductility compared to the brittle CCS mode.

The MC-FT failure mode, observed in the severely corroded beam (CS-20) and illustrated in Fig. 7(c), was characterized by progressive matrix cracking at the CFRP-concrete interface, ultimately leading to fiber tearing near the loading point. Unlike the other modes, no interface debonding or anchor pull-out was detected, with failure dominated by localized stress concentration within the CFRP sheet caused by extensive concrete cracking. The tearing of the CFRP sheet highlights the critical influence of material strength on the structural response under severe corrosion conditions, where stress concentration exacerbates localized failures.

4. Damage quantification in FRP-Strengthened corroded beams

4.1. Theories of damage mechanics

Damage mechanics is a theoretical framework that describes the gradual degradation of materials under loading. The concept was initially proposed by Kachanov in the 1950s, with the continuity factor (or damage variable) as its core, serving as a scalar measure of material damage. The damage index quantitatively describes the extent of damage in a material or structure, representing the transition from an undamaged state to complete failure. The damage index (*ID*) ranges from 0 to 1, where 0 indicates no damage and 1 represents complete failure. The index represents the proportion of residual strength or functionality of the material. Kachanov's theory is based on the concept of effective stress, defined as the average stress on the remaining cross-sectional area after considering

(a) CSS in Beam US-0

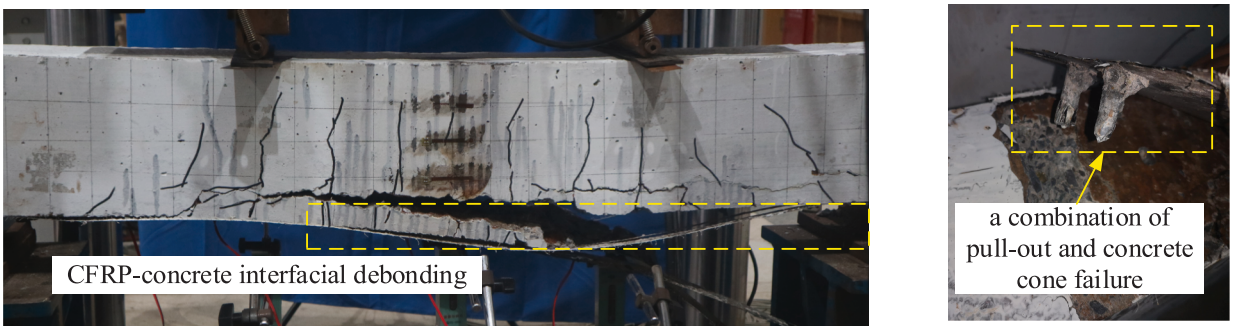

(b) CD-AP in Beam CS-10

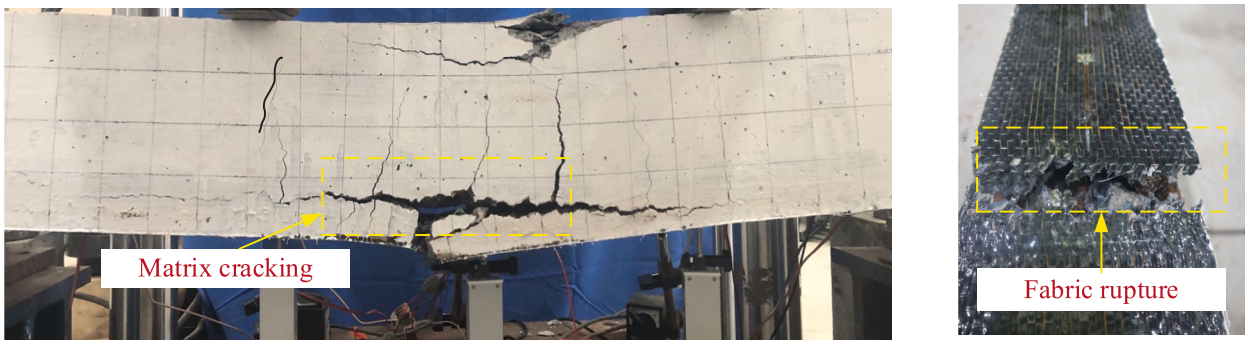

(c) MC-FT in Beam CS-20

Fig. 7. Modes of failure.

micro-level damage.

According to Kachanov's model, the damage index is defined as follows:

$$ID = 1 - \frac{\sigma_{effective}}{\sigma_{nominal}} \tag{2}$$

where $\sigma_{effective}$ represents the effective stress accounting for damage, and $\sigma_{nominal}$ denotes the original stress without considering damage.

In practical applications, particularly in complex engineering problems involving concrete and composite materials, the damage index is related to material properties, such as the cross-sectional area. If the original cross-sectional area of a material is A_0, and the effective cross-sectional area after loading or environmental influence is A_e, the damage index is expressed as follows:

$$ID = 1 - \frac{A_e}{A_0} = \frac{A_d}{A_0} \tag{3}$$

$$A_0 = A_e + A_d \tag{4}$$

where A_0 represents the initial total area, and A_e denotes the remaining effective area capable of bearing stress. When $A_0 = A_e$, no damage has occurred, resulting in $ID = 0$. Conversely, when $A_e = 0$, the material is completely destroyed, yielding $ID = 1$.

4.2. Improved damage assessment model

Cumulative AE ring-down count refers to the total number of AE signals generated over a specific period due to micro-damage events, including microcrack propagation, friction, and delamination. This parameter is used to quantify the damage state of materials under load. During experiments on reinforced concrete beams, AE sensors are installed to capture acoustic waves emitted by the concrete. The extent of damage in the beams can be assessed by analyzing wave characteristics such as amplitude, frequency, and count [41–44].

The damage assessment model for corroded RC beams reinforced with FRP can be improved by integrating AE technology with the damage index (*ID*). This approach considers the actual damage to the beam and its performance after reinforcement. The extent of structural damage can be quantified by establishing a relationship between the damage index and *AE* ring-down count. Typically, *ID* is determined by comparing the AE response count to a reference value, such as the count at complete failure. For example, *ID* can be defined as the ratio of the current cumulative *AE* ring-down count to a reference value, such as the count at complete failure.

Let N_m denote the cumulative *AE* ring-down count at complete failure of the entire *RC* beam, and N_d denote the cumulative count when the damage area reaches A_d. After *FRP* reinforcement, the load-bearing capacity and damage propagation pattern of the beam change. Consequently, $N_{m,F}$ is defined as the cumulative *AE* ring-down count at complete failure of the *FRP*-reinforced beam, while N_d,

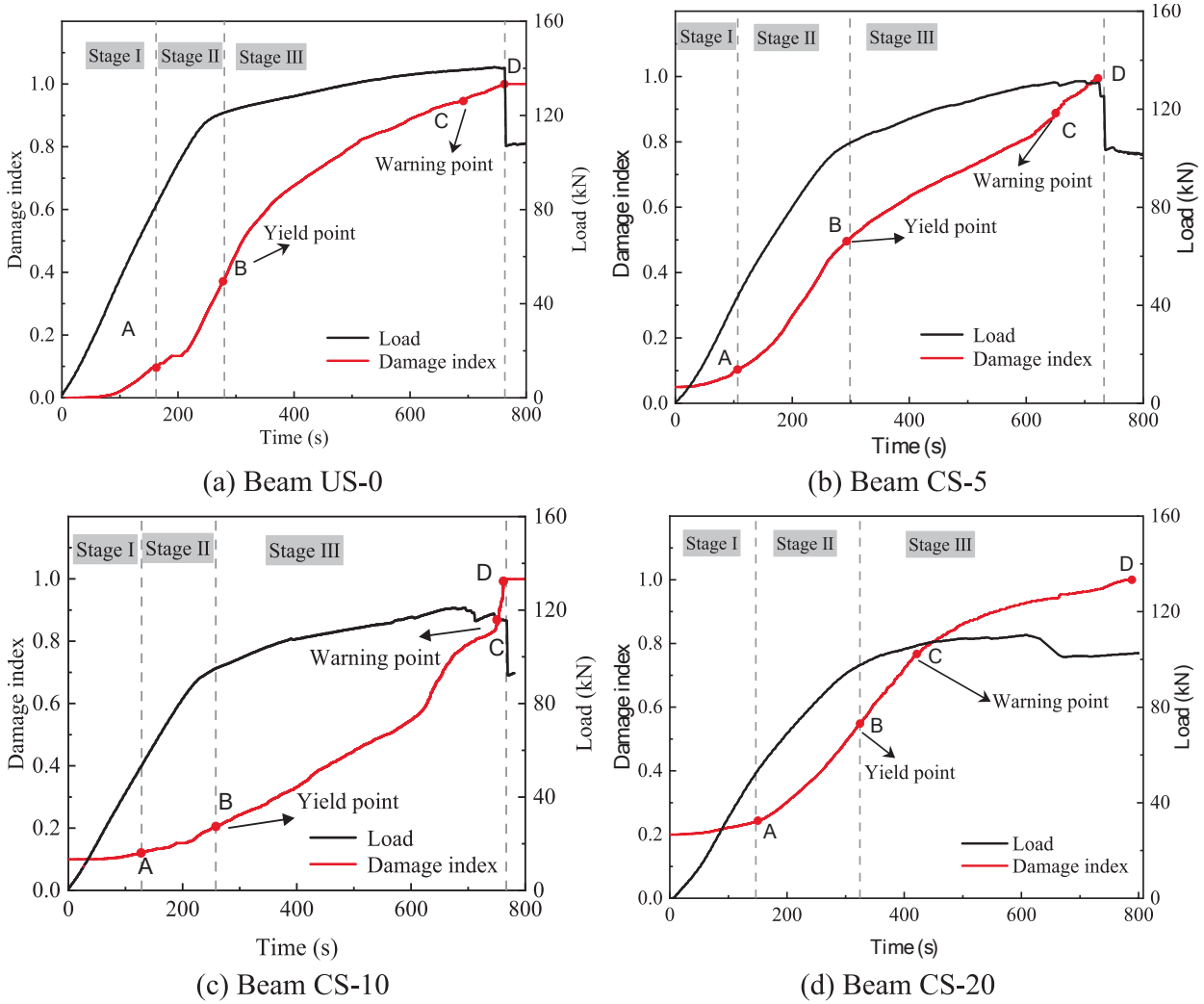

Fig. 8. Characteristics of damage index and load variation over time for test beam.

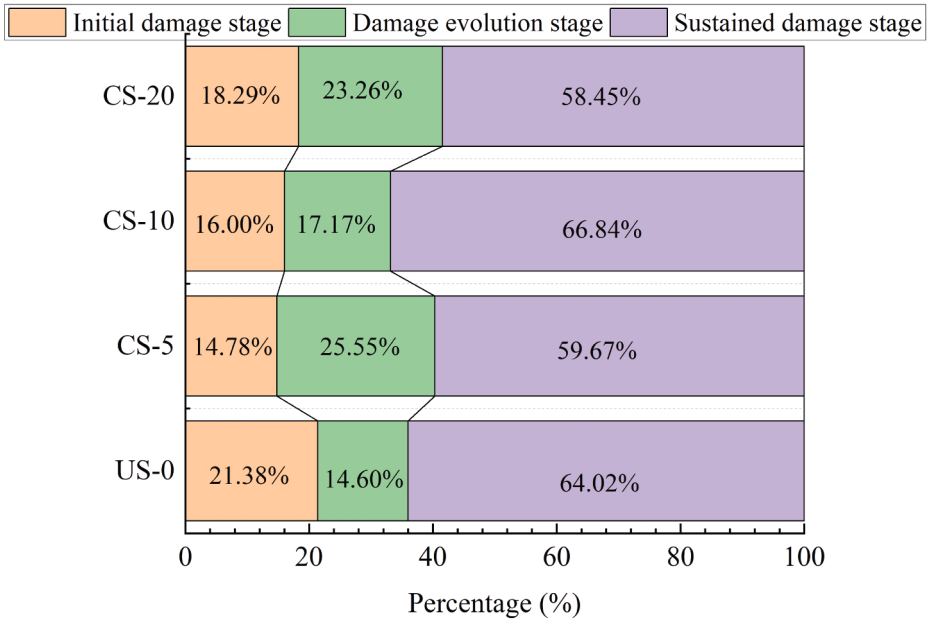

(a) Proportion of duration at different damage stages

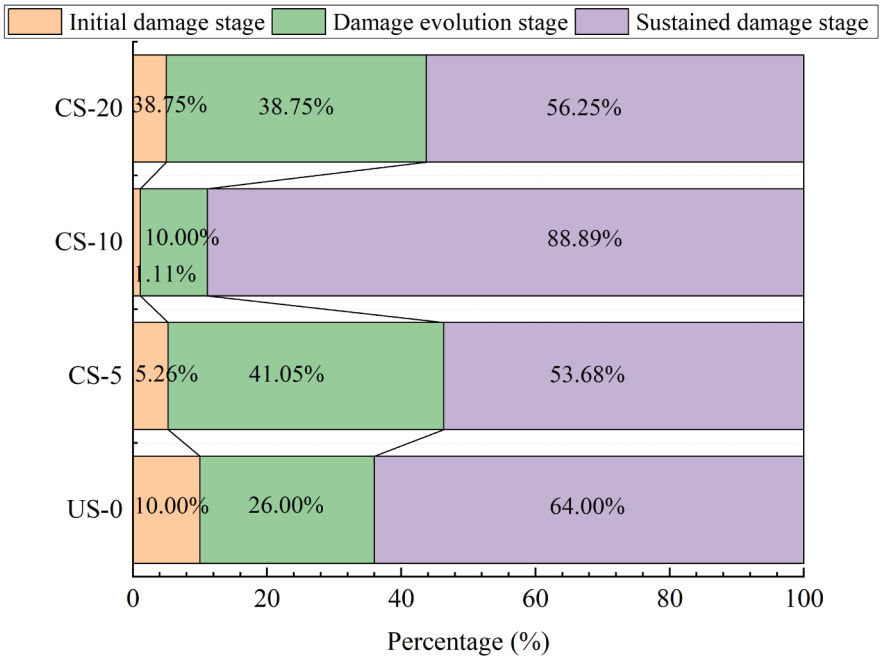

(b) Proportion of cumulative acoustic emission ring-down count at different damage stages

Fig. 9. Duration and cumulative acoustic emission ring-down count ratios for beams reinforced with a novel FRP anchoring system at different damage stages.

$_F$ represents the cumulative count when the same damage area A_d is reached after reinforcement.

$$ID_F = \frac{N_{d,F}}{N_{m,F}} \tag{5}$$

The initial damage index due to corrosion is considered. The effect of corrosion on the unreinforced beam is calculated using an equation, while accounting for the influence of *FRP* reinforcement on the corrosion process and the ultimate load-bearing capacity. For the *FRP*-reinforced beam, the initial damage index due to corrosion is redefined as $ID_{0,\ F}$:

$$ID_{0,F} = 1 - \frac{F_{d,F}}{F_{0,F}} \tag{6}$$

where $F_{d,F}$ and $F_{0,F}$ represent the ultimate load-bearing capacity of the corroded and uncorroded beams after *FRP* reinforcement, respectively.

The damage index *ID* should be adjusted to reflect the actual condition of the *FRP*-reinforced beam, considering the effects of reinforcement:

$$ID = ID_{0,F} + (1 - ID_0)\frac{N_{d,F}}{N_{m,F}} \tag{7}$$

5. Fractal theory-based damage early warning for FRP-strengthened corroded beams

5.1. Damage degree evaluation

Fig. 8 shows the relationship between the damage index and time for beams reinforced with a novel *FRP* anchoring system, with all four curves indicating a gradual increase in the damage index. Key milestones in damage progression are marked on the damage index–time curve, representing the damage states of the test beam at various stages. Points A, B, and D are identified based on the cumulative acoustic emission ring-down count and the load–deflection relationship of the *RC* beam during loading. Point C is determined through fractal feature analysis. Point A (initial damage onset) marks the initial rapid increase in the acoustic emission ring-down count, indicating the onset of early damage. Point B (Yield point): Corresponds to the yield load of the reinforced concrete beam, as identified from the load–deflection curve. This point reflects the onset of significant crack propagation caused by reinforcement yielding. Point C (early warning), identified through fractal dimension analysis, serves as an early warning of the critical transition to structural failure, aiding in damage control. Point D (ultimate failure) corresponds to the ultimate failure of the test beam, when the structure loses its primary load-bearing capacity.

The damage progression of the test beam is divided into three stages. The initial damage stage (before point A) is characterized by the formation and gradual accumulation of structural damage. The damage evolution stage (between points A and B) involves pronounced damage that accelerates with increasing load. Finally, the sustained damage growth stage (between points B and D) sees rapid damage expansion, ultimately leading to the loss of structural functionality.

Fig. 9 presents the duration and cumulative AE ring-down count ratios for beams reinforced with a novel FRP anchoring system at different damage stages. The initial damage stage corresponds to early crack development, characterized by limited AE signals and a low overall damage level. Minor changes during the initial damage phase are crucial for predicting the structure's long-term performance. The duration ratios differ significantly across varying corrosion levels. The duration ratios are 21.38 % for beam US-0, 14.78 % for beam CS-5, 16.00 % for beam CS-10, and 18.29 % for beam CS-20. This indicates that the initial phase is shortest for beam CS-5, suggesting a relationship between corrosion level and crack development rate. The AE ring-down count ratios are 10.00 % for beam US-0, 5.26 % for beam CS-5, 1.11 % for beam CS-10, and 5.00 % for beam CS-20. In contrast, a higher number of microcracks under severe corrosion conditions contributed to increased AE signals for beam CS-20. Moderate corrosion may inhibit microcrack formation during the initial damage phase, while severe corrosion exacerbates it.

During the damage evolution stage, the AE ring-down count significantly increases under all conditions, indicating increased crack activity. The ring-down count ratio for beam CS-5 is the highest at 41.05 %, possibly indicating rapid crack development under 5 % corrosion. Beam CS-20 has the highest duration ratio at 23.26 %, suggesting the damage evolution stage is prolonged under severe corrosion, with visible crack formation and expansion. This phenomenon indicates that as the degree of corrosion increases, the FRP anchoring system is subjected to a higher risk of damage.

The sustained damage growth stage begins with the yielding of the reinforcement and continues until the ultimate structural failure. During this stage, the load on the structure increases, accelerating damage progression. Beams CS-10 and US-0 exhibit the highest sustained damage growth ratios in this stage, at 66.84 % and 64.02 %, respectively. Beam CS-10 shows the highest AE ring-down count ratio, reaching 88.89 %. This may indicate the most frequent and intense AE activity for moderately corroded beams during this stage, suggesting significant structural weaknesses. The AE ring-down counts for beams CS-5 and CS-20 are 59.67 % and 58.45 %, respectively, implying a lower degree of damage during the sustained damage growth stage under mild and severe corrosion.

In summary, corrosion degree is closely related to damage development behavior. Limited AE signals during the initial damage stage indicate low damage, while the significant increase during the damage evolution and sustained growth stages suggests increasing structural damage. These changes are strongly associated with the level of corrosion, reflecting the varying behavior of the FRP anchoring system under different corrosion conditions.

5.2. Theory of fractals and correlation dimension

Fractal theory characterizes complex systems using statistical scaling laws—rather than single integer dimensions—and has been extensively applied in nonlinear mechanics and solid-state physics. Since AE signal parameters such as energy and ringing counts also exhibit fractal self-similarity, fractal analysis has become an effective tool for monitoring damage evolution in materials [33–35]. Based on the fundamental principle of scale measurement, fractal theory is represented by the following formula.

Measuring a line segment of length L with a scale r yields:

$$N(r) \times r^1 = L \tag{8}$$

Similarly, for the area S of a planar figure and the volume V of a solid figure, measurements using scales r^2 and r^3, respectively, yield the following results:

$$N(r) \times r^2 = S \tag{9}$$

$$N(r) \times r^3 = V \tag{10}$$

These can be unified as:

$$N(r) \times r^d = C \tag{11}$$

where C is the physical property of the geometric shape, and d is the topological dimension.

In traditional Euclidean space, dimensions are integers, while the fractal dimension (FD) is a non-integer and can be determined as follows:

$$FD = \frac{ln(C/N(r))}{lnr} \tag{12}$$

The calculation yields:

$$ln(N(r)) = FD \times ln\left(r^{-1}\right) + ln(C) \tag{13}$$

The box-counting method is a common approach for calculating fractal dimension. It involves covering an image with boxes of size r and counting the number of non-empty boxes $N(r)$ intersecting the image. The fractal dimension is obtained by plotting $\ln(N(r))$ against $\ln(r^{-1})$ on a log–log graph and determining the slope of the resulting line. This method is suitable for measuring the fractal dimension of planar shapes, typically ranging from 0 to 2.

The concept of correlation dimension was introduced by Grassberger and Procaccia [45]. It has since been widely applied due to its ease of extraction from experimental data. This measure considers N points in a spatial set A, each represented by its coordinates. Two points are considered correlated if their distance is less than a threshold δ. The correlation dimension is defined as the proportion of point pairs satisfying the correlation condition.

$$C(\delta) = \frac{1}{N^2}\sum\nolimits_{i,j=1}^{N} \theta\left(\delta - \left|x_i - x_j\right|\right) \tag{14}$$

where $\theta(r)$ is the Heaviside function.

$$\theta(r) = \begin{cases} 0, u < 0 \\ 1, u \geq 0 \end{cases} \tag{15}$$

The correlation dimension can be expressed as:

$$D = -\lim_{\delta \to 0} \frac{ln(C(\delta))}{ln\delta} \tag{16}$$

Based on experimental data collected from the complete failure process of reinforced concrete beams using acoustic emission, the correlation dimension of the chaotic time series of acoustic emission parameters was calculated using a program.

5.3. Phase space reconstruction of AE parameter time series

5.3.1. Phase space reconstruction

Phase space reconstruction is a key method in acoustic emission time series analysis for recovering the dynamic characteristics of a chaotic system from a single output time series. This method reveals the chaotic attractor, representing specific trajectories in the chaotic system.

In this study, the coordinate delay method was used for phase space reconstruction of the time series. This approach sets different time delays to convert a one-dimensional time series into a multi-dimensional phase space. This transformation captures the dynamic behavior of the system.

$$X_{(i)} = \left[x_{(i)}, x_{(i+1)}, \cdots, x_{(i+(m-1)t)}\right] \tag{17}$$

5.3.2. Determination of time delay τ

The accurate reconstruction of a system's phase space relies on selecting an appropriate time delay τ, which governs the independence and informational quality of the reconstructed coordinates. If τ is too small, redundancy between coordinates increases, resulting in the loss of essential dynamical features. Conversely, a large τ weakens the causal relationships among coordinates, distorting the phase space and masking the system's intrinsic behavior. Therefore, τ must be optimized to balance redundancy and independence, ensuring the reconstructed space accurately reflects the system's dynamics.

To identify the optimal time delay τ, the study employed the C–C method developed by H. S. Kim [46], a robust approach grounded in the principles of autocorrelation and correlation integrals. The method evaluates nonlinear dependencies within a time series by calculating the correlation integral $C(m,N,r,\tau)$, which quantifies the fraction of point pairs within a defined distance rrr in an embedded phase space. The correlation integral is expressed as:

$$C(m,N,r,\tau)=\frac{2}{N_m^2}\sum\nolimits_{1\le i<j\le N_m}H\left(r-\|x_i-x_j\|\right) \tag{18}$$

where $H(a)$ represents the Heaviside function, N_m is the number of embedded points, and $\|x_i - x_j\|$ denotes the maximum norm separation between points.

The nonlinear dependency is measured using the statistic $S(m,N,r,\tau)$, defined as the difference between two correlation integrals:

$$S(m,N,r,\tau)=C(m,N,r,\tau)-C^m(1,N,r,\tau) \tag{19}$$

The optimal time delay τ is identified by minimizing the variation in $S(m,r,\tau)$ across multiple scales of r. Specifically, the C–C method evaluates the statistical variation $\Delta S(m,t)$:

$$\Delta S(m,t)=max\{S(m,r_j,\tau)\}-min\{S(m,r_j,\tau)\} \tag{20}$$

Here, representative values of r_j are selected, typically 0.5σ,1.0σ,1.5σ, and 2.0σ, where σ is the standard deviation of the dataset. By averaging $\Delta S(m,t)$ across embedding dimensions mmm (ranging from 2 to 7), the C–C method calculates:

$$\Delta\overline{S}(\tau)=\frac{1}{6}\sum\nolimits_{m=2}^{7}\Delta S(m,\tau) \tag{21}$$

The first local minimum of $\Delta\overline{S}(\tau)$ is considered the optimal time delay. This point represents the balance where spatial components achieve relative independence while minimizing statistical variation. Selecting the first minimum avoids redundancy caused by overly small τ values, while preventing loss of dynamical information associated with excessively large τ values. In this study, the C–C method was applied to analyze the time series data of the four test beams. As shown in Fig. 10, the variation $\Delta\_S(\tau)$ reached its first minimum at $\tau = 3$, which was therefore adopted as the optimal delay time for phase space reconstruction.

5.3.3. Determining the embedding dimension m

The embedding dimension mmm is a critical parameter in phase space reconstruction, as it determines the number of dimensions required to fully characterize the dynamics of a time series. A dimension that is too low fails to capture the system's complexity, resulting in incomplete reconstruction and loss of dynamic information. Conversely, an excessively high dimension introduces redundancy and increases computational costs. Thus, selecting the minimum embedding dimension that preserves the system's essential dynamics is imperative. In this study, the saturated correlation dimension method was employed to determine the optimal embedding dimension for the AE time series. The method evaluates the behavior of the correlation dimension D as mmm increases. When D stabilizes and no longer exhibits significant change, the corresponding embedding dimension is considered sufficient for

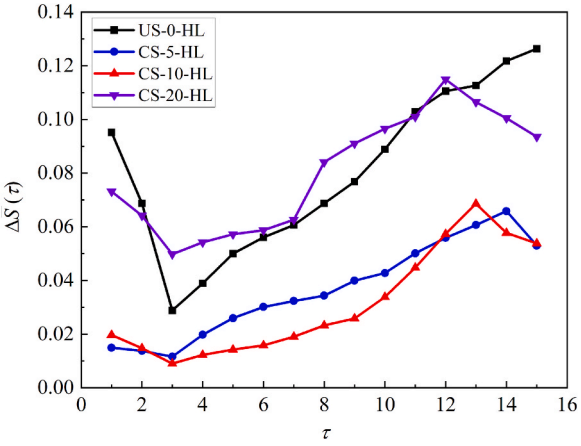

Fig. 10. $\tau - \Delta\_S(\tau)$ relationship curves.

reconstructing the phase space.

The relationship between the correlation dimension D and embedding dimension mmm is illustrated in Fig. 11. Initially, D increases with mmm, reflecting the addition of dynamic information as the dimensionality expands. However, as mmm continues to grow, D approaches a plateau, indicating that the system's underlying structure has been effectively captured. In this study, when the embedding dimension lies between 3 and 5, the curve exhibits steady growth, where the slope of D with respect to mmm becomes negligible. Based on these observations, the embedding dimension mmm was set to 4, striking a balance between reconstruction accuracy and computational efficiency. This choice ensures that the phase space adequately reflects the intrinsic dynamics of the AE signals while avoiding unnecessary computational overhead.

5.4. Damage early warning and fractal analysis of reinforced beams based on acoustic emission

5.4.1. G-P algorithm for correlation dimension

The Grassberger-Procaccia (G-P) algorithm, a foundational approach for quantifying fractal characteristics in nonlinear systems, was employed to determine the correlation dimension of AE time series [47]. This method enables the assessment of system complexity by reconstructing the phase space and analyzing its structural behavior. Here, the AE signals collected during the four-point bending tests of FRP-strengthened corroded RC beams were analyzed to reveal the progressive nature of crack evolution.

To reconstruct the phase space from the one-dimensional AE time series $X=\{x_1, x_2, \ldots, x_n\}$, the time delay τ and embedding dimension m must first be established. Using the C–C method, optimal values for these parameters were determined. The phase space vectors were then reconstructed as follows:

$$X_i = \left[x_i, x_{i+t} \cdots x_{i+(m-1)t}\right] \; i = 1, 2, \cdots, N_m \tag{22}$$

where $N_m = n-(\mathrm{m}-1)\tau$ is the total number of reconstructed vectors. The embedding process transforms the time series into an mmm-dimensional space, preserving the system's underlying dynamics while capturing its geometric complexity.

The correlation function $W(r)$, which measures the number of vector pairs X_i and X_j within a given distance r, is expressed as:

$$W(r(k)) = \frac{1}{{N_m}^2} \sum_{i=1}^{N_m} \sum_{j=1}^{N_m} H\left[r - \|X_i - X_j\|\right] \tag{23}$$

where $H(u)$ is the Heaviside function defined as:

$$H(u) = \begin{cases} 0, u < 0 \\ 1, u \geq 0 \end{cases} \tag{24}$$

The Euclidean distance $\|X_i - X_j\|$ quantifies the spatial separation between reconstructed vectors X_i and X_j in the phase space. Within the scaling region, $W(r)$ follows a power-law relationship with the distance r:

$$W(r) \sim r^D$$

where D represents the correlation dimension—a measure of the fractal complexity of the system. By taking the logarithm of both sides, the correlation dimension can be determined as the slope of the linear region in the log–log plot of $W(r)$ versus r:

$$D = -\lim_{r \to 0} \frac{\ln W(r(k))}{\ln r(k)} \tag{25}$$

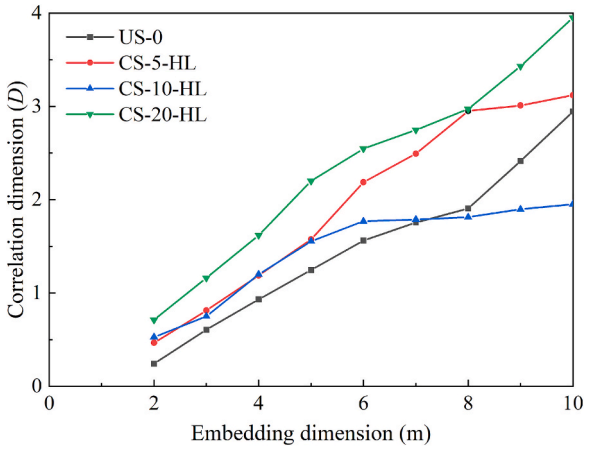

Fig. 11. Relationship curve between correlation dimension d and embedding dimension m.

The slope is extracted using the least-squares fitting method, ensuring robust estimation of the correlation dimension within the identified scaling region.

The *G-P* algorithm was implemented in Python to normalize acoustic emission time series parameters, perform phase space reconstruction, and calculate the correlation dimension during the bending of reinforced concrete beams.

5.4.2. Correlation dimension characteristics of acoustic emission parameters

Using the *C–C* method, the damage index was divided into 20 groups ranging from 0 % to 100 %, each covering a 5 % increment (e.g., 0 %–5%, 5 %–10 %). This approach provides a detailed analysis of structural integrity evolution during loading. The fractal dimension *D* of each group was calculated using Python to understand the complex behavior of acoustic emission (*AE*) events in compressed samples. The analysis aimed to determine whether AE ring-down counts exhibited fractal characteristics during loading. These characteristics would indicate complex, self-similar patterns of crack propagation and damage accumulation in concrete beams.

Fig. 12 shows representative ln(*r*) versus ln(*W*(*r*)) curves for the tested beams. These curves are crucial for understanding the fractal nature of AE data, reflecting AE events' fractal behavior and used to calculate the fractal dimension. Correlation coefficients derived from these graphs quantitatively evaluate the quality of the fractal analysis.

Table 4 details the minimum and average correlation coefficients (R_{min} and R_{av}) for each beam. These coefficients are key indicators of the reliability of fractal analysis. Values closer to 1.0 indicate a stronger statistical relationship, thereby enhancing the reliability of fractal dimension interpretation. The average correlation coefficient R_{av} for each beam exceeded 0.93, while the minimum correlation coefficient R_{min} exceeded 0.83. These high values indicate a significant correlation between the logarithmic transformation of r and AE event counts, confirming the self-similar nature of the AE data. This correlation emphasizes that the AE parameter series exhibits self-similarity during different damage stages of RC beams. This finding implies that despite the chaotic nature of crack propagation and material failure, AE data exhibit an underlying fractal structure. This fractal structure could be used to predict the progression of damage and impending failure of beams, providing a powerful tool for structural health monitoring.

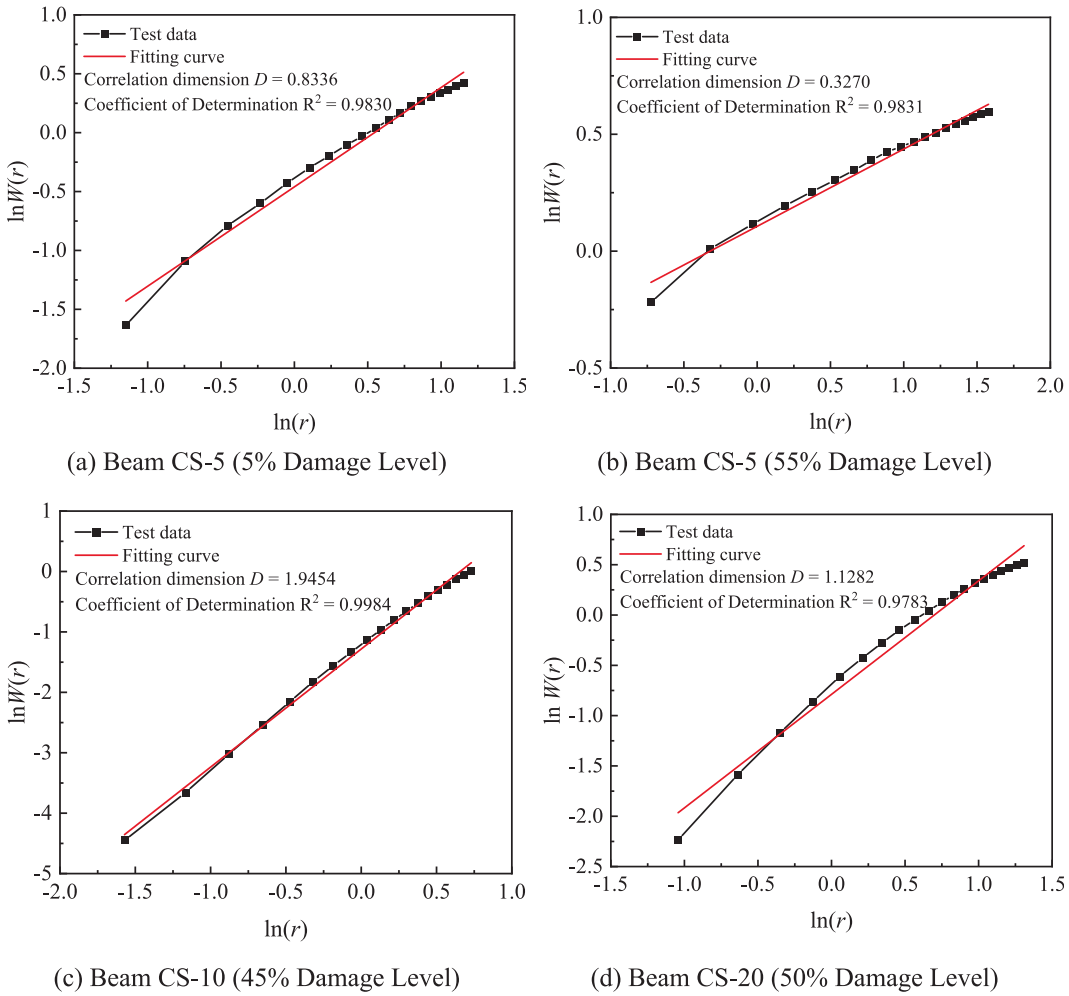

Fig. 12. Typical ln(*r*)–ln(*W*(r)) Curves of the Test Beams.

Table 4
Minimum and Average Correlation Coefficients.

Specimen	US-0	CS-5	CS-10	CS-20
R_{min}	0.8357	0. 8421	0.9697	0.8498
R_{av}	0.9352	0.9389	0.9868	0.9402

5.4.3. Damage early earning for reinforced beams based on AE correlation dimension

The correlation dimension D serves as an indicator of the internal mechanical properties and damage variations in reinforced beams. Statistically, the correlation dimension is inversely proportional to the degree of order within the dataset. A higher correlation dimension indicates a more disordered dataset, reflecting the uncertainty and randomness in microcrack formation, damage to FRP materials, and crack propagation direction and location. Conversely, a lower correlation dimension implies increased predictability and consistency in damage and crack propagation. Fig. 13 shows the relationship between the correlation dimension *D* and the damage index for corroded beams with a novel FRP anchoring system.

For the uncorroded reinforced beam (US-0), as the damage index increases from 0.05 to 0.25, the correlation dimension decreases from 1.00 to 0.57, with the lowest value of 0.24 occurring at a damage index of 0.20. This downward trend suggests that early microcracks are developing, but their impact on structural integrity is not yet significant. These early cracks remain stable, not leading to increased complexity in AE activity. As the damage index increases from 0.25 to 0.90, the correlation dimension rises, reaching a peak of 1.75. This sharp rise indicates accelerated internal damage, including crack propagation, coalescence, and large-scale failure of the FRP-substrate interface. At this point, structural stability declines rapidly, with damage transitioning from localized to widespread. After the damage index reaches 0.90, the correlation dimension quickly drops from a peak of 1.75 to 0.52. This rapid decrease reflects the structure entering a severe damage stage, where FRP delamination and structural cracking severely compromise load-bearing capacity and stability.

For the beam with 5 % corrosion (CS-5), as the damage index increases from 0.15 to 0.45, the correlation dimension decreases from 0.80 to 0.30, showing a fluctuating downward trend. This may indicate that internal damage has stabilized locally or crack propagation has been restricted. At a damage index of 0.45, the correlation dimension rises to 0.43, suggesting nonlinear damage progression and increased complexity. As the damage index increases from 0.45 to 0.80, the correlation dimension rises, reaching a peak of 0.93. This suggests widespread delamination or large-scale debonding of the FRP layer. These conditions lead to complex and frequent AE events, often due to stress concentration and sustained loading. After the damage index exceeds 0.80, the correlation dimension declines to 0.42 at a damage index of 1. This trend suggests that the FRP-reinforced structure, after experiencing complex damage, has lost most or all of its load-bearing capacity.

For the beam with 10 % corrosion (CS-10), as the damage index increases from 0.15 to 0.20, the correlation dimension rises to 1.20, indicating the initial effects of corrosion. Corrosion of reinforcement leads to volume expansion and increased internal stresses, causing microcracks at the concrete interface. As the damage index decreases from 0.25 to 0.35, the correlation dimension drops from 0.86 to 0.26, indicating a slowdown in crack development or temporary stabilization of damage. During this stage, the FRP anchoring system maintains structural integrity and slows damage spread. Between damage indices of 0.35 and 0.80, the correlation dimension rises significantly to 1.75. This peak indicates further failure of anchoring points, leading to extensive FRP delamination or rupture. As the damage index reaches 1.00, the correlation dimension drops to 0.55, suggesting that the structure has approached a failure state due to corrosion cracks. At this stage, the effectiveness of FRP reinforcement has significantly decreased, severely compromising structural integrity and stability.

For the beam with 20 % corrosion (CS-20), at a damage index of 0.25, the correlation dimension is relatively high (1.40). This indicates that even at the initial damage stage, corrosion has significantly impacted the FRP-reinforced beam by promoting microcrack formation and propagation. The increase in the correlation dimension from 0.94 at a damage index of 0.30 to 1.24 at 0.45 suggests nonlinear damage development. This fluctuation may be due to stress changes induced by corrosion, with damage developing at different rates in various regions as stress redistributes. At a damage index of 0.60, the correlation dimension sharply increases to 1.95, suggesting major structural changes, such as small-scale FRP debonding. At a damage index of 0.70, the correlation dimension reaches a peak of 2.30, indicating a severe damage state with extensive FRP debonding and significant damage at anchoring locations. As the damage index approaches 1.00, the correlation dimension remains high (1.80), indicating that the structure has entered a pre-failure state, with significantly reduced stability.

The correlation dimension D of the acoustic emission signal is a key parameter, with peak point C indicating the imminent failure of each test beam. After this peak, the correlation dimension sharply declines until significant damage or ultimate failure of the FRP-reinforced beam occurs. This trend reveals the gradual internal failure of the reinforced beam, primarily due to three factors: (a) Rapid Microcrack Development**:** An increase in the correlation dimension indicates rapid microcrack propagation, suggesting a more complex internal failure process, with damage spreading from the microscopic to the macroscopic level. (b) Interface Failure**:** In the FRP anchoring system, bond interface failure between the FRP and the substrate manifests as greater complexity and irregularity in the acoustic emission signals, increasing the correlation dimension. (c) Stress Concentration**:** Stress concentrates near FRP anchors or existing cracks, where material failure is more severe, resulting in increased acoustic emission activity.

For beam US-0, the correlation dimension peaked at 1.5 at a damage index of 0.90, then dropped to 1.1 as damage progressed. For the other three beams, with lower damage indices (0.80, 0.80, and 0.70), the correlation dimension peaks reached 0.93, 1.75, and 2.3, respectively. This indicates that with increasing corrosion levels, the damage index at the early warning point decreases, and the correlation dimension peak appears earlier. The earlier warning point, especially for beams in highly corrosive environments, suggests

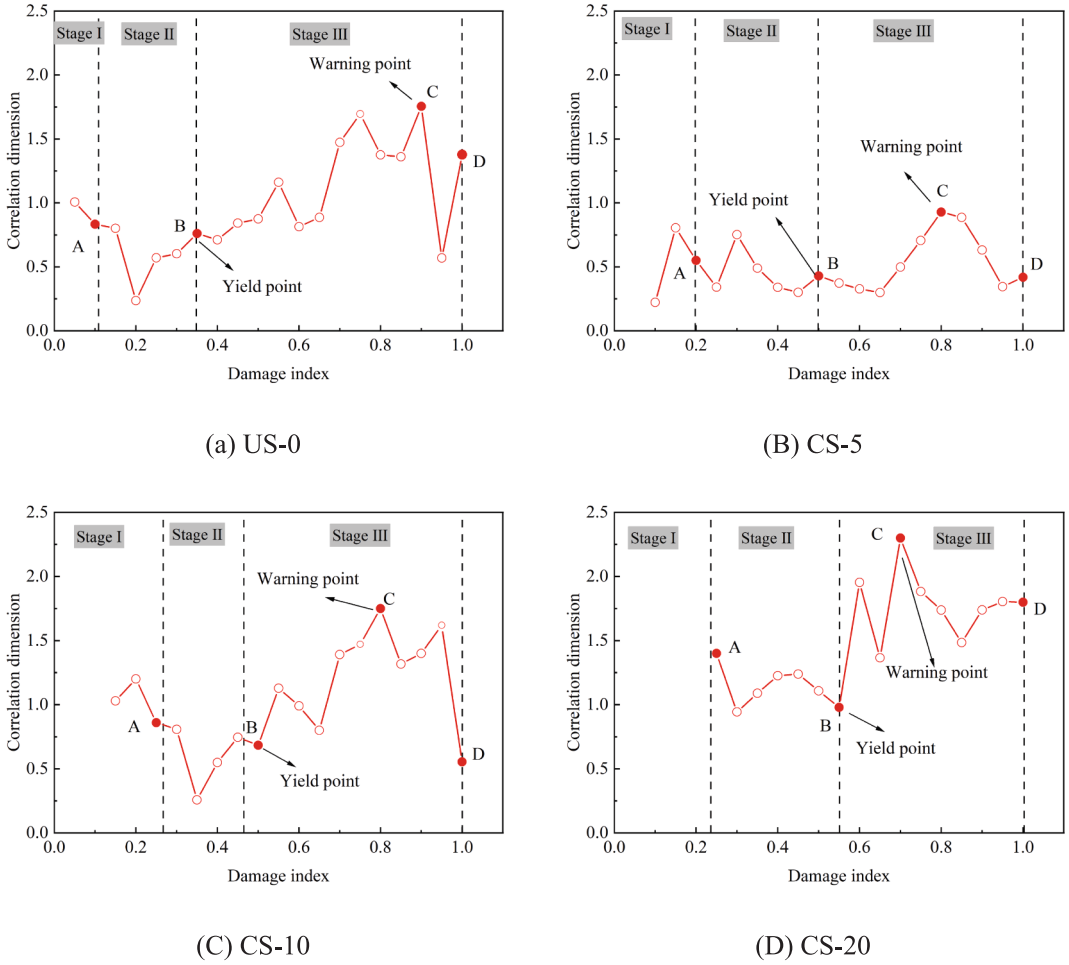

Fig. 13. Correlation dimension-damage index curve for test beams.

that corrosion accelerates damage progression, affecting the performance of the FRP anchoring system. These observations highlight the importance of considering environmental factors in FRP reinforcement design, supporting the development of more effective structural health monitoring strategies.

6. Conclusion

This study presents a novel approach that combines AE monitoring with fractal analysis to evaluate and predict damage progression in FRP-strengthened RC corroded beams. The main conclusions of the study are as follows:

(1) A damage model was developed that elucidates the characteristic stages of structural damage in FRP-strengthened RC beams, revealing three distinct phases: initial damage, damage evolution, and sustained growth. The model effectively tracks damage progression under various corrosion conditions, with results showing that corrosion accelerates both the accumulation and rate of damage. In environments with moderate to severe corrosion, AE ring counts significantly increase, reflecting enhanced crack activity and a marked decline in the structural load-bearing capacity.

(2) The study demonstrates a clear relationship between the variation in correlation dimension and the degree of damage in the strengthened beams. Higher correlation dimensions are associated with more disordered internal damage, such as micro-crack propagation and material interface failure. A distinctive pattern of correlation dimension evolution was observed, with an initial rise followed by a decrease as the damage index increases, signaling the transition from early-stage damage to advanced degradation.

(3) The findings indicate that corrosion accelerates the damage process, with the correlation dimension reaching its peak at lower damage indices. This suggests that corrosion not only induces damage but also hastens its progression, making early detection and intervention critical. As corrosion severity increases, the damage warning threshold lowers, underscoring the rapid and significant impact of corrosion on structural integrity.

(4) The use of fractal analysis, particularly through monitoring the correlation dimension, provides an effective and reliable method for assessing damage in real-time. The correlation dimension serves as an early warning indicator, allowing for more accurate and timely detection of damage, particularly in environments where corrosion is prevalent.

CRediT authorship contribution statement

Tanbo Pan: Writing – review & editing, Methodology, Investigation, Conceptualization. **Xubing Xu:** Writing – original draft, Methodology, Investigation. **Yonglai Zheng:** Methodology, Investigation. **Liangqin Wu:** Methodology, Investigation. **Chao Yang:** Methodology, Investigation. **Beyazit Bestami Aydin:** Methodology, Investigation. **Yang Li:** Methodology, Investigation. **Yubao Zhou:** Methodology, Investigation.

Declaration of competing interest

The authors declare that they have no known competing financial interests or personal relationships that could have appeared to influence the work reported in this paper.

Acknowledgments

The authors acknowledge financial support from the National Natural Science Foundation of China (No. 52468023), the Early-Career Young Scientistsand Technologists Project of Jiangxi Province (No. 20244BCE52161), and the Natural Science Foundation of Jiangxi Province, Youth Program (No. 20252BAC200092).

Data availability

Data will be made available on request.

References

[1] Song Y, Wightman E, Kulandaivelu J, Bu H, Wang Z, Yuan Z, et al. Rebar corrosion and its interaction with concrete degradation in reinforced concrete sewers. Water Res 2020;182.
[2] Hou L, Zhou B, Guo S, Aslani F, Chen D. Corrosion behavior and flexural performance of reinforced concrete/ultrahigh toughness cementitious composite (RC/UHTCC) beams under sustained loading and shrinkage cracking. Constr Build Mater 2019;198:278–87.
[3] Zhang R, Castel A, Francois R. Concrete cover cracking with reinforcement corrosion of RC beam during chloride-induced corrosion process. Cement Concrete Res 2010;40:415–25.
[4] Qin SD, Dirar S, Yang J, Chan AHC, Elshafie M. CFRP shear strengthening of reinforced-concrete T-beams with corroded shear links. J Compos Constr 2015;19.
[5] El-Maaddawy T, Nessabi A, El-Dieb A. Flexural response of corroded reinforced concrete beams strengthened with powder-actuated fastened composites. J Compos Constr 2013;17.
[6] Papakonstantinou CG, Balaguru PN, Auyeung Y. Influence of FRP confinement on bond behavior of corroded steel reinforcement. Cement Concrete Comp 2011;33:611–21.
[7] Malumbela G, Moyo P, Alexander M. Load-bearing capacity of corroded, patched and FRP-repaired RC beams. Mag Concrete Res 2011;63:797–812.
[8] Soudki KA. FRP repair of corrosion-damaged concrete beams - Waterloo experience. Solid Mech Appl 2006;140:165–73.
[9] Al-Rousan RZ, Issa MA. The effect of beam depth on the shear behavior of reinforced concrete beams externally strengthened with carbon fiber-reinforced polymer composites. Adv Struct Engng 2016;19:1769–79.
[10] Sun W, Jirsa JO, Ghannoum WM. Behavior of anchored carbon fiber-reinforced polymer strips used for strengthening concrete structures. ACI Mater J 2016;113:163–72.
[11] Dong K, Gao Y, Yang S, Yang Z, Jiang J. Experimental investigation and analytical prediction on bond behaviour of CFRP-to-concrete interface with FRP anchors. Case Stud Constr Mat 2023;19.
[12] Ke Y, Zhang SS, Smith ST, Yu T. Novel embedded FRP anchor for RC beams strengthened in flexure with NSM FRP bars: concept and behavior. J Compos Constr 2023;27.
[13] Muciaccia G, Khorasani M, Mostofinejad D. Effect of different parameters on the performance of FRP anchors in combination with EBR-FRP strengthening systems: a review. Constr Build Mater 2022;354.
[14] Ozbakkaloglu T, Fang C, Gholampour A. Influence of FRP anchor configuration on the behavior of FRP plates externally bonded on concrete members. Engng Struct 2017;133:133–50.
[15] Smith ST, Rasheed HA, Kim SJ. Full-range load-deflection response of FRP-strengthened RC flexural members anchored with FRP anchors. Compos Struct 2017;167:207–18.
[16] Degala S, Rizzo P, Ramanathan K, Harries KA. Acoustic emission monitoring of externally bonded FRP-reinforced concrete. Proc SPIE 2008;6935.
[17] Zhang FQ, Yang YG, Fennis SAAM, Hendriks MAN. Developing a new acoustic emission source classification criterion for concrete structures based on signal parameters. Constr Build Mater 2022;318.
[18] Zhao WC, Wang ZZ, Song ZL, Ranjith PG, Zhang H, Wang TT. Experimental exploration of damage propagation in rocks using acoustic emission. B Eng Geol Environ 2021;80:6065–75.
[19] Zhao YF, Ren S, Wang L, Zhang P, Liu R, Chen F, et al. Acoustic emission and physicomechanical properties of concrete under sulfate attack. J Mater Civil Eng 2021;33.
[20] Zhou XH, Shan WC, Liu JP, Li J. Fracture characterization of composite slabs with different connections based on acoustic emission parameters. Struct Control Hlth 2021;28.
[21] Pan TB, Shu ZJ, Liu YC, Aydin BB, Li Y, Zhou YJ, et al. Acoustic emission based health monitoring of RC corroded beams strengthened by CFRP anchorage system under bending loads. Compos Struct 2025;372.
[22] Pan TB, Zheng YL, Zhou YB, Luo WB, Xu XB, Hou CY, et al. Damage pattern recognition for corroded beams strengthened by CFRP anchorage system based on acoustic emission techniques. Constr Build Mater 2023;406.
[23] Pan TB, Zheng YL, Zhou YJ, Liu YC, Yu KL, Zhou YB. Coupled effects of corrosion damage and sustained loading on the flexural behavior of RC beams strengthened with CFRP anchorage system. Compos Struct 2022;289.

[24] Ma G, Li H, Zhou WS, Xian GJ. Acoustic emission monitoring of concrete columns and beams strengthened with fiber reinforced polymer sheets. Proc SPIE 2012; 8347.
[25] Nair A, Cai CS. Acoustic emission monitoring of bridges: review and case studies. Engng Struct 2010;32:1704–14.
[26] Ma G, Wu C. Crack type analysis and damage evaluation of BFRP-repaired pre-damaged concrete cylinders using acoustic emission technique. Constr Build Mater 2023;362.
[27] Ma G, Wu C, Hwang H-J, Li B. Crack monitoring and damage assessment of BFRP-jacketed concrete cylinders under compression load based on acoustic emission techniques. Constr Build Mater 2021;272.
[28] Liu J, Fan X, Shi C. Effect of bonding layers on dynamic fracture characteristics of FRP reinforced concrete. Constr Build Mater 2021;309.
[29] Du F, Li D, Li Y. Fracture mechanism and damage evaluation of FRP/steel-concrete hybrid girder using acoustic emission technique. J Mater Civil Eng 2019;31.
[30] Carpinteri A, Lacidogna G, Niccolini G. Fractal analysis of damage detected in concrete structural elements under loading. Chaos Soliton Fract 2009;42: 2047–56.
[31] Hao QS, Shen Y, Wang Y, Zhang X. A fractal model of acoustic emission signals in sliding friction. Tribol Lett 2019;67.
[32] Lyu Q, Tan JQ, Zhou JP, Ranjith PG, Hu CE, Luo WB. Fractal characteristics and acoustic emission of a low-clay shale after CO2-water-rock interactions. Deep Rock Mech: Res Eng. 2019:201-6.
[33] Michallek F, Dewey M. Fractal analysis of the ischemic transition region in chronic ischemic heart disease using magnetic resonance imaging. Eur Radiol 2017; 27:1537–46.
[34] Tan JQ, Xie J, Li L, Lyu Q, Han JQ, Zhao ZG. Multifractal analysis of acoustic emissions during hydraulic fracturing experiments under uniaxial loading conditions: a niutitang shale example. Geofluids 2020.
[35] Wang YS, Liu J. Fractal analysis of damage detected by acoustic emissions in prestressed reinforced concrete beam under loading. Aer Adv Eng Res 2016;30: 295–9.
[36] Ye C, Xie H, Wu F, Hu J, Ren L, Li C. Asymmetric failure mechanisms of anisotropic shale under direct shear. Int J Rock Mech Min 2024;183.
[37] Kong X, Zhan M, Lin H, Cai Y, Ji P, He D, et al. Time-varying characteristics of acoustic emission and fractals based on information dimension during structural failure of coal subjected to uniaxial compression. Measurement 2024;236.
[38] Yang H, Wang E, Wang X, Song Y, Chen D, Wang D, et al. Predicting the failure of rock using critical slowing down theory on acoustic emission characteristics. Engng Fail Anal 2024;163.
[39] Yu JG, Ziehl P, Zárate B, Caicedo J. Prediction of fatigue crack growth in steel bridge components using acoustic emission. J Constr Steel Res 2011;67:1254–60.
[40] Selman E, Ghiami A, Alver N. Study of fracture evolution in FRP-strengthened reinforced concrete beam under cyclic load by acoustic emission technique: an integrated mechanical-acoustic energy approach. Constr Build Mater 2015;95:832–41.
[41] Saliah SNM, Nor NM, Abd Rahman N, Abdullah S, Tahir MS. Evaluation of severely damaged reinforced concrete beam repaired with epoxy injection using acoustic emission technique. Theor Appl Fract Mec 2021;112.
[42] Prem PR, Verma M, Ambily PS. Damage characterization of reinforced concrete beams under different failure modes using acoustic emission. Structures 2021; 30:174–87.
[43] Ming P, Lu J, Liu MY, Cai X, Chen XD. Quantitative statistical analysis of the crack propagation and fracture process of self-compacting rubber concrete based on acoustic emission. Struct Control Hlth 2021;28.
[44] Pan TB, Zhang ZX, Zheng YL, Wang K. Acoustic emission-based analysis of mechanical behavior and damage evolution in corroded RC square columns. Constr Build Mater 2025;469.
[45] Grassberger P, Procaccia I. Estimation of the Kolmogorov-entropy from a chaotic signal. Phys Rev A 1983;28:2591–3.
[46] Kim HS, Eykholt R, Salas JD. Nonlinear dynamics, delay times, and embedding windows. Physica D 1999;127:48–60.
[47] Zheng YL, Wen Y, Pan TB, Liu YC, Zhou YJ, Li RZ, et al. Fractal characteristics and damage evaluation of corroded beams under four-point bending tests based on acoustic emission techniques. Measurement 2022;202.